Solution conformations of three small cluster oligosaccharide mimetics (SCOM) from D-glucosamine, D-altrosamine, and (-)-quinic acid

Quy L. Nguyen, Laura Olmstead, Sandeep Bains, and Andreas H. Franz*

Department of Chemistry, University of the Pacific, Stockton, CA 95211, USA,
E-mail: afranz@pacific.edu

Dedicated to Dr. Paul H. Gross on the occasion of his 76th birthday

Abstract

Three small cluster oligosaccharide mimetics were synthesized, and their $CDCl_3$ solution conformations were determined with NMR experiments. In this paper, we confirmed conformational similarities in rings A and B in all three compounds, and we provide the overall solution geometries. In all cases, an unusual cyclohexane *twist-boat* conformation with long-range ^4J-(W)-coupling was observed. The origin of the bias towards the *twist-boat* was attributed primarily to the fused ring system between the cyclohexane ring and the dioxacyclopentane (acetal) including hydrogen bonding. Temperature-annealed molecular dynamics simulations complemented the NMR experiments and supported the overall assignment.

Keywords: Oligosaccharide mimetic, NMR, NOE difference spectroscopy, conformational analysis

Introduction

Quinic acid (**1**, Figure 1)[1] and its derivative shikimic acid (**2**, Figure 1)[2-4] (from *Illicium japonica* and *floridanum*) are key intermediates during the biochemical synthesis of essential aromatic amino acids, such as L-tryptophan, L-phenylalanine, and L-tyrosine in plants, bacteria, and fungi as well as building blocks for folic acid, alkaloids, and vitamins. The quinic acid/shikimic acid pathway does not exist in mammals, which has led to extensive research activities geared towards the development of suitable antibiotic therapeutics.[5,6] Especially the conversion of 3-dehydroquinic acid (DHQ) to 3-dehydroshikimic acid (DHS) has been recognized as an effective target for inhibition in plants. Several commercial herbicides selectively inhibit the DHQ-DHS conversion and prevent growth of weeds. However, disruption of the DHQ-DHS

pathway by shikimic acid derivatives (**3**, Figure 1) has also recently been shown to cause therapeutic inhibition of *Mycobacterium tuberculosis*.[7]

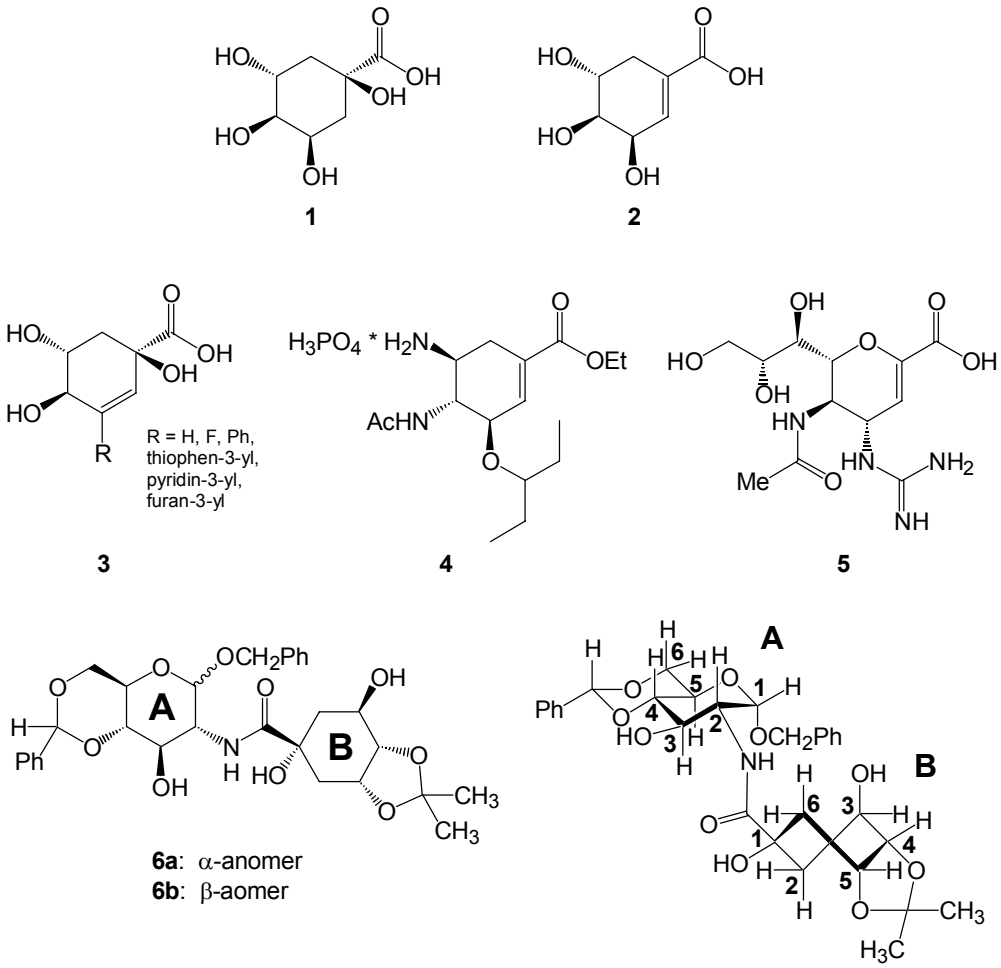

Figure 1. Chemical structures of quinic acid (**1**), shikimic acid (**2**). Compounds **3**,[7] **4** (Tamiflu™, Roche)[8], and **5** (Relenza™, Glaxo-Smith)[9,10] show anti-influenza activity. Compound **6** has been previously synthesized in our laboratory.[13]

Derivatives of shikimic acid have been used to inhibit other biochemical pathways for example the infectious pathway of the influenza virus (common flu). Potent anti-influenza A+B effect has been observed for derivatives of shikimic acid[7] inhibiting viral neuraminidase. The widely-prescribed anti-flu medication Tamiflu™ (Oseltamivir, Roche, **4**, Figure 1)[8] is not only effective in treating common flu strains, but it has also been used successfully in the treatment of the bird (avian) flu in laboratory animals. Contrary to animal experiments, Tamiflu's™ effectiveness in humans infected with the H5N1 flu strain is still controversial because only a few studies with limited statistical value have been conducted, and the understanding of the drug's action against the virus is only rudimentary. Tamiflu™ is thought to act as influenza virus

neuraminidase inhibitor with the possibility of alteration of virus particle aggregation and release. The less well-known Relenza™ (Zanamivir, GlaxoSmithKline, **5**, Figure 1)[9,10] is also an effective inhibitor of common flu strains by the same mechanism. The problem of a sufficient supply of these two drugs in case of an influenza pandemic and the necessity for a continuous search for new structural analogs has been discussed in the literature.[11,12]

Therefore, all analogs of shikimic and quinic acid such as compound **6** (Figure 1)[13] and analogs thereof have to be considered potentially valuable bioactive compounds, and their exact structural characterization is of great importance. In this paper, we discuss the NMR-spectroscopic properties and solution conformation of the quinic acid derivative **6** and two new structural analogs thereof (**16** and **17**).

Results and Discussion

Synthesis of quinic amides and NMR analysis

The α- and β-anomers of compound **6** (Figure 1) had previously been synthesized and characterized by NMR in our laboratory (Table 1).[13] Commercially available D-(-)-quinic acid was concurrently dehydrated and iso-propylidenated in acetone in the presence of *p*-toluenesulfonic acid to yield (1R,3R,4R,5R)-1,3-dihydroxy-4,5-*O*-isopropylidene-1-carboxy cyclohexane 1,3-lactone (quinic acid lactone **7**).[14] The lactone was subsequently opened nucleophilically with benzyl-2-amino-4,6-*O*-benzylidene-2-deoxy-α/β-D-glucopyranoside to yield **6a** and **6b**. We have previously shown that the cyclohexane ring in quinamide such as compound **6** (Figure 1) exists to a significant extent in the *twist*-boat conformation in $CDCl_3$. This was concluded from the existence of a long-range ^4J-coupling constant between $H2b^B$ and $H4^B$ (W-coupling) as well as small gauche couplings of 2.7 Hz for both $H5^B/H6a^B$ and $H5^B$/H6bB indicating that the C-$H5^B$ single bond was dissecting the $H6a^B$-C-$H6b^B$ bond angle. Our assignment of ring A was supported by large coupling constants between $H2^A/H3^A$, $H3^A/H4^A$, and $H4^A/H5^A$ consistent with the *trans*-fused dioxa-decaline system.[13]

To investigate whether the *twist*-boat conformation in **6** is the result of the large glycosyl substituent or merely a result of the fusion between the six-membered cyclohexane ring and the five-membered isopropylidene acetal ring, we synthesized compound **8** from quinic lactone **7** through ring opening in methanolic ammonia at 100 ºC for 2 d (Scheme 1). Compound **8** was obtained in 100 % yield with NMR purity after evaporation of the solvent.

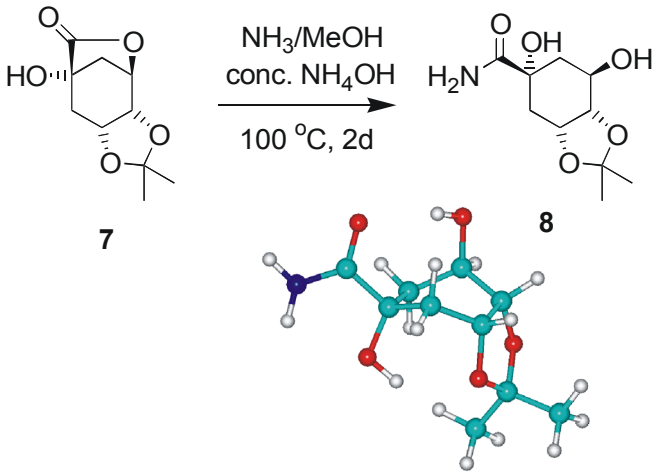

Scheme 1. Synthesis of compound **8**. The most stable conformation *in vacuo* for **8** is shown which was consistent with all observed *J*-values and NOEs (temperature annealed molecular dynamics simulations, AM1, 600 K → 0 K).

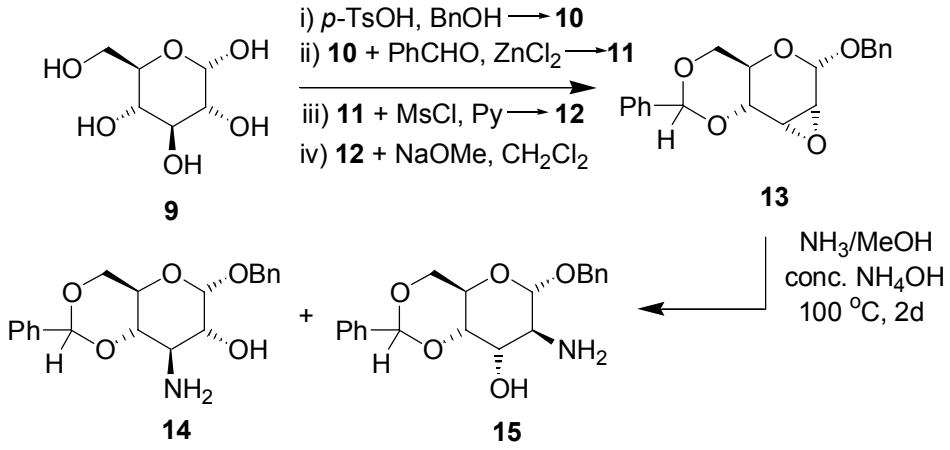

Scheme 2. Synthesis of compounds **16** and **17**. The preparation of **14** and **15** has been reported in the literature.[15]

The synthesis of **16** and **17** from α-benzyl-3-amino-3-deoxy-4,6-*O*-benzylidene-D-glucopyranoside **14** and α-benzyl-2-amino-2-deoxy-4,6-*O*-benzylidene-D-altropyranoside **15**, respectively, is shown in Scheme 2. Compounds **14** and **15** were obtained after treatment of D-glucose **9** with benzyl alcohol in the presence of toluenesulfonic acid.[15] The benzyl glucoside **10** was 4,6-*O*-benzylidenated (**11**) with benzaldehyde in the presence of $ZnCl_2$ and was subsequently converted into the 2,3-di-*O*-mesylate **12**. Compound **12**, upon treatment with NaOMe in CH_2Cl_2, yielded the 2,3-anhydro-allopyranoside **13**, which was opened under elevated pressure in MeOH saturated with NH_3. Diastereoselectivity was high in favor of the *altro*-configuration (**14**:**15** ratio 1:25) consistent with the Fuerst-Plattner rule of *trans*-diaxial opening of the epoxide.[16-18]

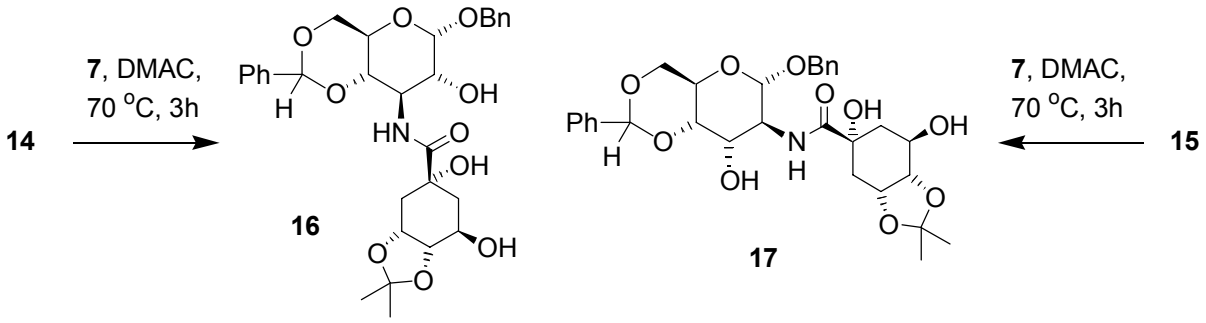

Scheme 3. Nucleophilic opening of quinic lactone with **14** and **15**.

The quinic acid lactone was opened nucleophilically by both **14** and **15** with minimal solvent to yield **16** (65% yield) and **17** (60% yield) as shown in Scheme 3. The mixture of **16** and **17** was observed to crystallize from *N*,*N*-dimethylacetamide during the reaction, which was attributed primarily to the high melting point of **16** compared to **17** (218-220 ºC and 105-107 ºC, respectively).

Overall structure determination and NOE-difference experiments

The cyclohexane ring B of **6** had been shown[13] by analysis of ^3J-values to exist to a significant extent in an unusual *twist*-boat solution conformation in $CDCl_3$ in both anomers (Table 1). However, the exact overall solution conformation of the whole molecule had not been determined and only minimal molecular modeling data were discussed.

We determined NOE difference spectra for several proton pairs in **6a**. To establish a set of reference buildup curves, we chose the benzylidene CH-resonance with *trans*-annular spin-exchange to H-4 and H-6a in ring A. The benzylidene CH-proton is located in a *trans*-dioxa-decaline system, in which minimal conformational flexibility can be assumed. The mixing time was varied, and the NOE enhancements were integrated relative to the irradiated proton, and the values were plotted against τ_{mix} to generate buildup curves. The NOE buildup followed a standard saturation profile and an initial slope = $0.035*10^{-3}$ s^{-1} was determined for CHPh/H-6a. This slope served as a reference for all other NOE buildup experiments.

We subsequently investigated $H1^A$ and its position relative to $H2^A$ and the amide NH-proton. The NOEDIF spectrum after irradiation of H1 is shown in Figure 2a. Significant NOE signals were observed at $H2^A$ and at the amide NH but also at the benzylic CH_2-protons and the phenyl ring. The corresponding buildup curves (Figure 2b) resulted in slopes for $H2^A$, CH_2aPh, CH_2bPh, NH, and H^{arom} of $0.043*10^{-3}s^{-1}$, $0.003*10^{-3}s^{-1}$, $0.026*10^{-3}s^{-1}$, and $0.005*10^{-3}s^{-1}$, respectively.

In the β-anomer (**6b**), the same set of proton pairs was investigated with the slope of CHPh/H-6a being $0.023*10^{-3}s^{-1}$ and resulted in slopes for $H3^A$, $H5^A$, CH_2bPh, NH, and H^{arom} of 0.008, 0.064, 0.022, 0.010, and 0.009, respectively.

Table 1. ^{1}H-NMR data for compound **6**.[13] The spectra were recorded in $CDCl_3$ at rt. "nr" = not resolved

	6a	**6b**
	δ [ppm], *J* [Hz]	δ [ppm], *J* [Hz]
1^A	4.91 (d) $^3J_{1,2}$=3.3	4.72 (d) $^3J_{1,2}$=8.1
2^A	4.19 (dt) $^3J_{2,1}$=3.9 $^3J_{2,3}$=9.9 $^3J_{2,NH}$=9.9	3.68 (ddd) $^3J_{2,1}$=8.1 $^3J_{2,3}$=9.6 $^3J_{2,NH}$=7.2
3^A	4.00 (t) $^3J_{3,2}$=9.3 $^3J_{3,4}$=9.3	4.05 (dd) $^3J_{3,2}$=9.9 $^3J_{3,4}$=9.0
4^A	3.59 (t) $^3J_{4,3}$=9.0 $^3J_{4,5}$=9.0	3.59 (t) $^3J_{4,3}$=9.0 $^3J_{4,5}$=9.0
5^A	3.90 (dt) $^3J_{5,4}$=9.9 $^3J_{5,6a}$=4.5 $^3J_{5,6b}$=9.9	3.47 (dt) $^3J_{5,4}$=9.6 $^3J_{5,6a}$=9.6 $^3J_{5,6b}$=4.8
$6a^A$	3.76 (t) $^3J_{6a,5}$=9.9 $^3J_{6a,6b}$=9.9	3.82 (t~dd) $^3J_{6a,5}$=9.9 $^3J_{6a,6b}$=10.5
$6b^A$	4.25 (dd) $^3J_{6b,5}$=4.5 $^3J_{6b,6a}$=9.9	4.37 (dd) $^3J_{6b,5}$=4.5 $^3J_{6b,6a}$=10.5
$OH2^A$	-	-
$OH3^A$	3.11 (s, br)	3.00 (s)
NH	~7.4 (nr)	7.29 (d) $^3J_{NH,2}$=7.8
CHPh	5.56 (s)	5.55 (s)
CH_2Ph	4.55 (d)	4.61 (d)
	4.74 (d) ^2J=12.0	4.89 (d) ^2J=11.7
$H2a^B$	2.00 (dd) $^3J_{2a,3}$=3.3 $^2J_{2a,2b}$=15.0	2.01 (dd) $^3J_{2a,3}$=3.0 $^2J_{2a,2b}$=15.0
$H2b^B$	2.15 (ddd) $^4J_{2b,4}$=0.9 $^3J_{2b,3}$=5.7 $^2J_{2b,2a}$=14.7	2.20 (ddd) $^4J_{2b,4}$=0.9 $^3J_{2b,3}$=5.7 $^2J_{2b,2a}$=14.7
$H3^B$	~3.8 (nr)	~3.8 (nr)
$H4^B$	4.12 (ddd~dd) $^4J_{4,2b}$<1 $^3J_{4,3}$=3.3 $^3J_{4,5}$=6.6	4.12 (ddd~dd) $^4J_{4,2b}$<1 $^3J_{4,3}$=3.3 $^3J_{4,5}$=6.3
$H5^B$	4.54 (dt) $^3J_{5,4}$=6.3 $^3J_{5,6a}$=2.7 $^3J_{5,6b}$=2.7	4.53 (dt) $^3J_{5,4}$=6.9 $^3J_{5,6a}$=3.0 $^3J_{5,6b}$=3.0
$H6a^B$	2.14 (dd) $^3J_{6a,5}$=2.1 $^2J_{6a,6b}$=15.3	2.02 (dd) $^3J_{6a,5}$=3.6 $^2J_{6a,6b}$=15.3
$H6b^B$	2.42 (dd) $^3J_{6b,5}$=2.4 $^2J_{6b,6a}$=15.6	2.37 (dd) $^3J_{6b,5}$=2.7 $^2J_{6b,6a}$=15.9
$OH1^B$	3.53 (s)	Not ident.
$OH3^B$	4.39 (d) $^3J_{OH,3}$=3.6	Not ident.
$CH_3^{i\text{-}Pr}$	1.35 (s)	1.35 (s)
	1.53 (s)	1.52 (s)

The cyclohexane ring of 8 showed significant *twist*-boat conformation (Table 2). This was evident from the two small coupling constants (3.0 Hz) between H5 and H6a/b on the one side of the ring and from the small and medium *J*-value (2.7 Hz and 5.4 Hz) between H3 and H2a/b on the other side of the ring. In addition, a four-bond coupling of 1.8 Hz was observed between H4 and H2b. Without any substituent attached to the amide group, we concluded that the *twist*-boat conformation of derivatives such as **8** in $CDCl_3$ is caused by the fusion between the cyclohexane ring and the five-membered acetal ring. The *twist*-boat is additionally stabilized by a hydrogen bond between the amide group and OH3, which was inferred from NOE difference experiments (not shown) and temperature annealed molecular dynamics simulations (Scheme 1).

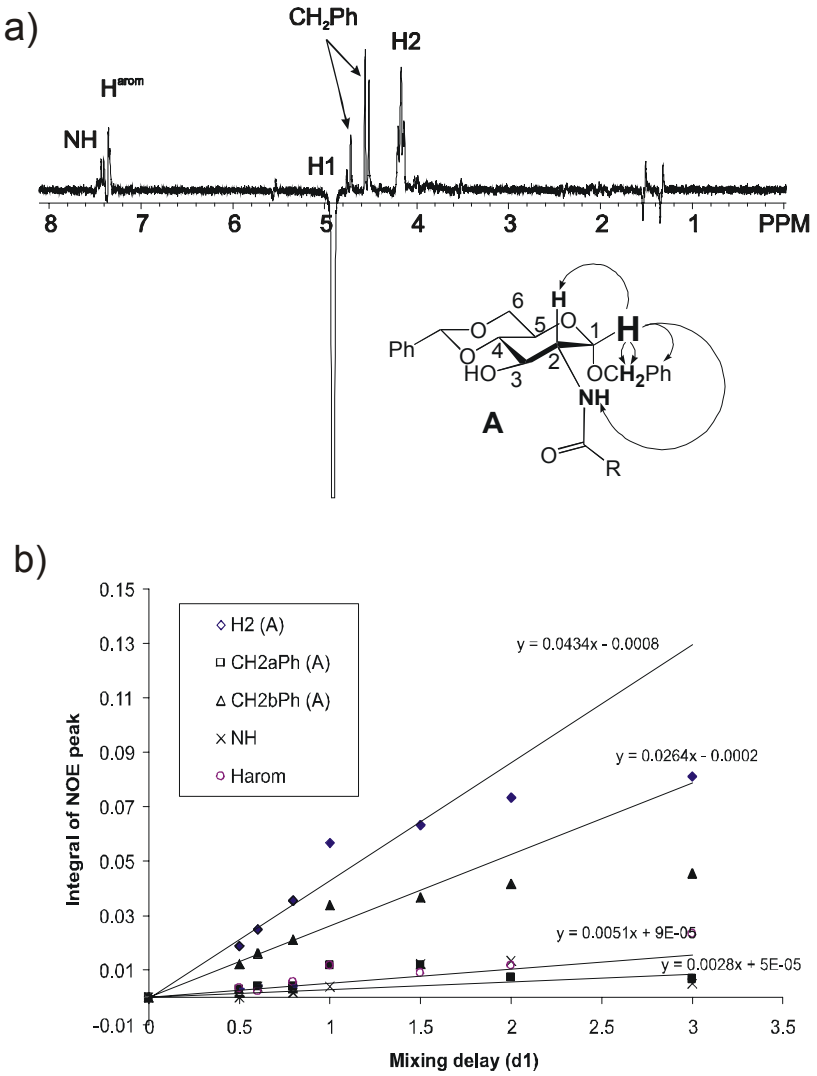

Figure 2. a) Selected NOEDIF spectrum of **6a** after irradiation of $H1^A$ at room temperature; b) NOEDIF buildup curves from arrayed mixing times.

Compound **16** with α-D-*gluco*-configuration displayed consistent coupling constants for a $^4C_1$ chair conformation in ring A (Table 2). The NMR signal of the anomeric proton showed a small gauche coupling of 3.6 Hz to H2, which in turn showed *trans*-diaxial coupling (9.9 Hz) to H3 and the same coupling to the OH-proton. Protons H3, H4, and H5 were characterized by large *trans*-diaxial coupling constants. Ring B displayed coupling features of a *twist*-boat conformation very similar to **8**. Also here, the four-bond coupling between H2bB and H4B was very distinct with 1.8 Hz as well as the bisecting gauche bond angle of H5 and the two geminal H6 protons (3.3 and 2.4 Hz).

Table 2. ^{1}H-NMR data for compounds **8**, **16**, and **17**. The spectra were recorded in $CDCl_3$ at rt. "nr" = not resolved

	8	**16**	**17**
	δ [ppm], *J* [Hz]	δ [ppm] , *J* [Hz]	δ [ppm] , *J* [Hz]
1^A	-	5.02 (d) $^3J_{1,2}$=3.6	4.81 (d~s) $^3J_{1,2}$<1
2^A	-	3.74 (dt) $^3J_{2,1}$=3.9 $^3J_{2,3}$=9.9 $^3J_{2,OH}$=9.9	~4.34 $^3J_{2,1}$=5.4 $^3J_{2,3}$= nr $^3J_{2,OH}$= nr
3^A	-	4.30 (ddd) $^3J_{3,2}$=9.9 $^3J_{3,4}$=10.5 $^3J_{3,NH}$=8.1	~4.09 $^3J_{3,2}$= nr $^3J_{3,4}$= nr $^3J_{3,OH}$= 6.9
4^A	-	3.60 (dd) $^3J_{4,3}$=9.6 $^3J_{4,5}$=10.5	3.69 (dd) $^3J_{4,3}$=3.0 $^3J_{4,5}$=9.9
5^A	-	3.93 (dt) $^3J_{5,4}$=9.6 $^3J_{5,6a}$=9.6 $^3J_{5,6b}$=4.5	~4.28 (nr)
$6a^A$	-	3.72 (t) $^3J_{6a,5}$=10.2 $^3J_{6a,6b}$=10.2	3.69 (dd) $^3J_{6b,5}$=3.0 $^3J_{6b,6a}$=9.9
$6b^A$	-	4.23 (dd) $^3J_{6b,5}$=4.8 $^3J_{6b,6a}$=10.2	4.41 (dd) $^3J_{6b,5}$=3.3 $^3J_{6b,6a}$=9.3
$OH2^A$	-	2.90 (d) $^3J_{OH2,2}$=10.5	-
$OH3^A$	-	-	3.04 (d) $^3J_{OH3,3}$=7.2
NH	6.95 (s); 5.61(s)	7.13 (d) $^3J_{NH,3}$=7.8	7.21 (d) $^3J_{NH,2}$=7.4
CHPh	-	5.50 (s)	5.65 (s)
CH_2Ph	-	4.79 (d)	4.79 (d)
		4.61 (d) ^2J=11.7	4.62 (d) ^2J=12.0
$H2a^B$	2.06 (dd) $^3J_{2a,3}$=2.7 $^2J_{2a,2b}$=15.0	2.02 (dd) $^3J_{2a,3}$=2.7 $^2J_{2a,2b}$=14.7	2.06 (dd) $^3J_{2a,3}$=3.0 $^2J_{2a,2b}$=15.0
$H2b^B$	2.30 (ddd) $^4J_{2b,4}$=1.8 $^3J_{2b,3}$=5.4 $^2J_{2b,2a}$=15.0	2.24 (ddd) $^4J_{2b,4}$=1.2 $^3J_{2b,3}$=5.1 $^2J_{2b,2a}$=14.7	2.25 (ddd) $^4J_{2b,4}$<1 $^3J_{2b,3}$=5.7 $^2J_{2b,2a}$=15.6
$H3^B$	3.85 (dt) $^3J_{3,2a}$=3.3 $^3J_{3,2b}$=6.9 $^2J_{3,4}$=3.3	3.81 (nr)	3.88 (nr)
$H4^B$	4.17 (ddd) $^4J_{4,2b}$=1.2 $^3J_{4,3}$=3.0 $^3J_{4,5}$=6.9	4.16 (ddd) $^4J_{4,2b}$=1.8 $^3J_{4,3}$=3.3 $^3J_{4,5}$=7.2	4.16(ddd~dd) $^4J_{4,2b}$<1 $^3J_{4,3}$=2.4 $^3J_{4,5}$=5.7
$H5^B$	4.60 (dt) $^3J_{5,4}$=6.9 $^3J_{5,6a}$=3.0 $^3J_{5,6b}$=3.0	4.58 (ddd~dt) $^3J_{5,4}$= nr $^3J_{5,6a}$= nr $^3J_{5,6b}$=3.3	4.58 (dt) $^3J_{5,4}$=5.7 $^3J_{5,6a}$=2.7 $^3J_{5,6b}$=2.7
$H6a^B$	2.14 (dd) $^3J_{6a,5}$=3.3 $^2J_{6a,6b}$=15.3	2.13 (dd) $^3J_{6a,5}$=3.3 $^2J_{6a,6b}$=15.6	2.07 (dd) $^3J_{6a,5}$=3.0 $^2J_{6a,6b}$=16.5
$H6b^B$	2.47 (dd) $^3J_{6b,5}$=2.7 $^2J_{6b,6a}$=15.9	2.47 (dd) $^3J_{6b,5}$=2.4 $^2J_{6b,6a}$=15.6	2.43 (dd) $^3J_{6b,5}$=1.8 $^2J_{6b,6a}$=15.6
$OH1^B$	3.41 (s)	3.43 (s)	3.57 (s)
$OH3^B$	4.43 (d) $^3J_{OH,3}$=3.9	4.43 (d) $^3J_{OH,3}$=4.2	~4.1 (d) $^3J_{OH,3}$=3.3
$CH_3^{i\text{-}Pr}$	1.37 (s)	1.35 (s)	1.36 (s)
	1.53 (s)	1.50 (s)	1.52 (s)

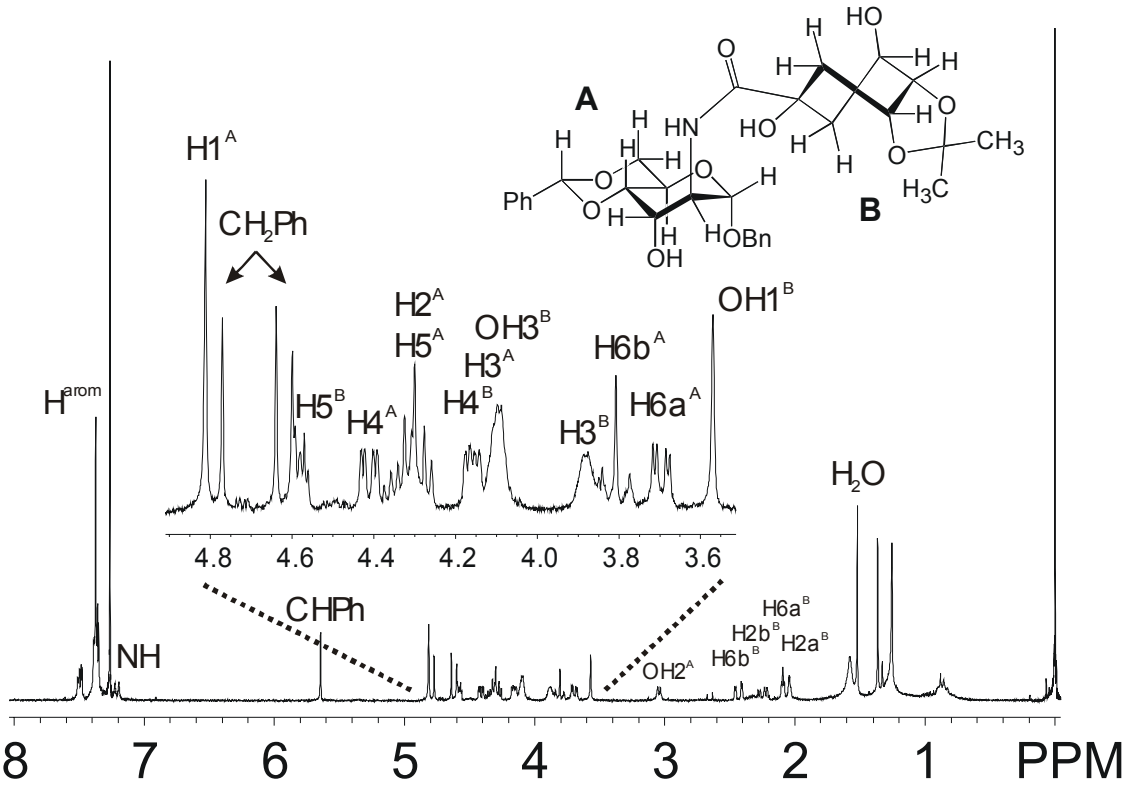

Figure 3. ^{1}H-NMR spectrum of **17** with assignments.

The *altro*-configuration of ring A in compound **17** manifested itself through small or not resolved coupling constants between $H1^{A}$, $H2^{A}$, and $H3^{A}$, followed by a double doublet for $H4^{A}$ with coupling constants of $^{3}J_{4,3}$ = 3.0 Hz and $^{3}J_{4,5}$ = 9.9 Hz (Figure 3, Table 2). Even though ring B represents a rather bulky substituent in axial position, it did not seem to affect the chair conformation in ring A to any significant extent. The coupling constants observed for the protons in ring B were very similar to those observed for both **8** and **16**, which implied the same *twist*-boat conformation. Compounds **16** and **17** were analyzed with NOE difference experiments in the same fashion. The fitting of the results to a structure determined from temperature annealed molecular dynamics simulation is described below.

Molecular dynamics simulations and geometry refinement with NOE data

After the experimental determination of NOE buildup curves for several proton pairs, we turned our attention to the computational description of both anomers of **6**. The molecular dynamics simulation of **6a** without dihedral angle restrictions and with temperature annealing from 600 K to 0 K resulted in the plot of selected *inter*-proton distances in Figure 4a. Uniform convergence of the proton distances to final 0 K values was observed with ring A in chair conformation and ring B in *twist*-boat conformation consistent with the *J*-coupling values. All temperature-averaged distances fall within the limit for reasonably strong NOE-signals (i.e. < 4Å) as experimentally observed. The final lowest energy structure is shown in Figure 4b with selected

inter-proton distances and averaged values in parentheses. The averaged distances were calculated from the first 30 ps of the trajectory at thermal equilibrium. Ring A and B were conformationally biased relative to each other through two hydrogen bonds at the amide carbonyl ($OH3^A$ and $OH3^B$). Table 3 shows the full list of *inter*-proton distances.

The temperature-averaged distance between CHPh and $H6a^A$ was 2.47 Å and was used as a reference distance for other *inter*-proton distances.

$$\frac{\text{Slope CHPh/H6a}^{\text{A}}\text{ buildup}}{\text{Slope H}^{\text{x}}/\text{H}^{\text{y}}\text{ buildup}} = \left(\frac{\text{Distance H}^{\text{x}} \rightarrow \text{H}^{\text{y}}}{\text{Distance CHPh} \rightarrow \text{H6a}^{\text{A}}} \right)^6 \quad (1)$$

a)

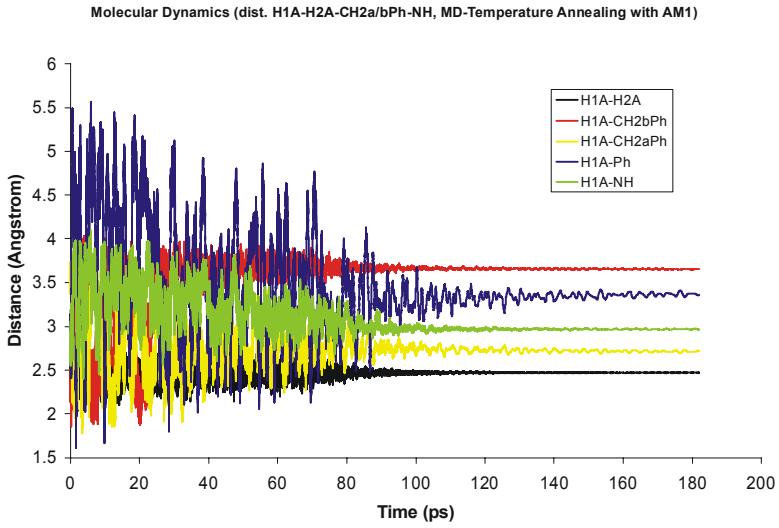

b)

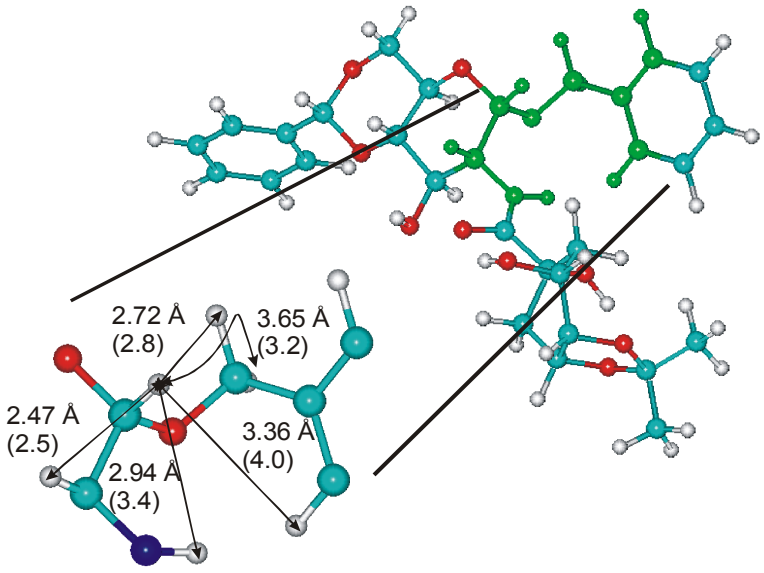

Figure 4. (a) Selected *inter*-proton distances from the 180 ps trajectory of **6a** during temperature annealing from 600 K to 0 K; (b) Lowest energy structure for **6a** with selected 0 K distances. High-temperature average distances from the first 30 ps of the trajectory are shown in parentheses.

Table 3. *Inter*-proton distances for **6a** and **6b** (in Å). The averaged values were obtained from the first 30 ps at thermal equilibrium. The distances determined from NOE experiments are shown with % errors in parentheses. n. o. = "not observed"

	H	**6a**			**6b**			**16**			**17**		
		0 K	TE	NOE	0 K	TE	NOE	0 K	TE	NOE	0 K	TE	NOE
	1-2	2.47	2.5	2.4(3)	3.14	3.1	-	2.45	2.4	2.5(4)	2.65	2.7	-
	1-3	3.97	-	-	2.81	-		3.88	-	n. o.	4.41	-	-
	1-5	3.65	-	-	2.45	-		3.68	-	n. o.	3.36	-	-
	1-CH_2a	3.65	3.2	3.4(6)	3.11	3.0	-	3.62	3.7	3.7(0)	2.67	2.7	-
A	1- CH_2b	2.72	2.8	2.6(6)	2.31	2.4	2.5(4)	2.72	2.7	2.5(7)	2.41	2.4	-
	4-CHPh	2.33	2.4	2.2(9)	2.33	2.3	2.0(14)	2.36	2.3	2.2(4)	2.34	2.4	2.7(12)
	6a-CHPh	2.47	2.5	Ref	2.47	2.5	Ref	2.47	2.5	Ref.	2.47	2.5	Ref.
	CHPh-Ph	3.11	3.1	2.5(18)	3.12	3.2	2.6(19)	3.17	3.3	2.8(15)	2.36	3.6	2.9(19)
	1-Ph	3.36	4.0	3.3(17)	4.52	4.5	2.9(35)	2.65	3.0	3.2(6)	4.83	4.4	-
	6b-4	3.17	3.2	3.5(12)	3.16	3.2	-	3.32	-	n. o.	3.30	-	3.6(9)
	6b-5	2.49	2.5	2.3 (7)	2.49	2.5	2.6(4)	2.44	2.4	2.5(4)	2.44	2.4	2.4(0)
B	6a-6b	1.82	1.8	1.9 (6)	1.82	1.8	1.9(5)	1.82	1.8	1.9(5)	1.82	1.8	1.9(5)
	3-OH3	2.81	2.6	4.0(42)	2.80	2.8	-	2.80	2.8	3.9(39)	2.81	2.8	-
	6b-OH3	2.04	2.4	3.2(36)	2.03	2.1	-	2.13	-	n. o.	2.13	-	3.0(42)
	NH-1^A	2.94	3.4	3.7(11)	2.52	3.0	2.8 (7)	5.19	5.5	n. o.	3.29	3.2	-
	NH-2^A	2.95	3.0	-	2.94	2.9	-	3.04	3.7	3.5(5)	2.95	2.9	-
	NH-$2a^B$	3.31	4.1	-	3.38	3.9	2.3(42)	3.61	-	n. o.	3.93	-	-
	NH-$2b^B$	3.90	4.4	-	3.94	4.3	-	3.97	-	n. o.	3.49	-	-
	NH-$6a^B$	4.00	3.1	-	3.94	4.0	-	3.72	-	n. o.	3.82	-	-
A/B	NH-$6b^B$	4.40	3.90	-	4.38	3.5	-	4.25	-	n. o.	4.28	-	n. o.
	NH-$OH1^B$	3.28	2.4	-	3.26	2.3	-	3.24	3.2	3.7(16)	3.26	3.3	4.0(21)
	NH-$OH3^B$	4.68	4.8	-	4.69	4.7	-	4.82	-	n. o.	4.77	-	-
	3^A-$OH3^B$	6.24	6.6	4.6(28)	6.18	6.1	-	4.55	-	-	6.21	-	-
	$OH3^A$-CO	2.47	4.9	-	2.33	2.4	-	2.31	-	-	5.07	-	-
	$OH3^B$-CO	2.13	2.1	-	2.13	2.1	-	2.21	-	-	2.21	-	-

Inter-proton distances can be approximated by their inverse sixth-power relationship to the rate of the experimentally observed NOE buildup (see experimental). Although this relationship is not free from errors, it frequently allows reasonable approximation of *inter*-proton distances with errors smaller than 10%. This equation can be solved for the distance between any H^x/H^y proton pair in **6a** if their NOE buildup curve can be determined and compared to the slope of the

reference pair CHPh/H6a^{A} and the respective distance between CHPh/H6a^{A} from the molecular dynamics simulation.

Several *inter*-proton distances in **6a** relative to the CHPh/H6a^{A} and their respective errors are shown in Table 1. In general, similar values or smaller errors were observed when the temperature-averaged distances from the molecular dynamics trajectory were used to match the NOEDIF data. However, several values deviated significantly more than 10% from the predicted values. For example, the distance determined for the H1^{A}/*ortho*-H^{arom} proton pair displayed a 17% error. Rotation of the phenyl ring causes significantly greater time-averaged distance than the 0 K structure suggests. In addition, ring current effects from the aromatic π-system can be expected to affect the efficiency of spatial spin density transfer and increase the error of measurement. The % error was particularly significant in the case for proton pairs that involved hydroxyl protons. Surprisingly, long-range spin density exchange between all hydroxyl protons was observed despite distances greater than 6Å. This observation was explained with partial hydration of the compound and a hydrogen bond network connecting remote OH-groups. In such water-bridged systems, the r^{-6}-relationship for NOEs does not apply strictly any more and larger distance errors can be expected. To find support for this explanation, the molecule should be computationally modeled in a water-box with molecular dynamics to reveal the existence of such water bridges. Such calculation was not attempted because of lack of computing power, and the structure shown in Figure 4b was assumed to resemble the $CDCl_3$ solution structure adequately.
The investigation of the solution conformation of the β-anomer **6b** was carried out in analogous fashion, and *inter*-proton distances are summarized in Table 1. Temperature-annealed molecular dynamics resulted in a smooth convergence to a 0 K structure and revealed a pair of hydrogen bonds across the amide bond including OH3^{A} and OH3^{B} (Figure 5a). The proposed conformation of **6b**, as shown in Figure 5b, supported our NOE data very well with identical *twist*-boat conformation in ring B compared to **8**.

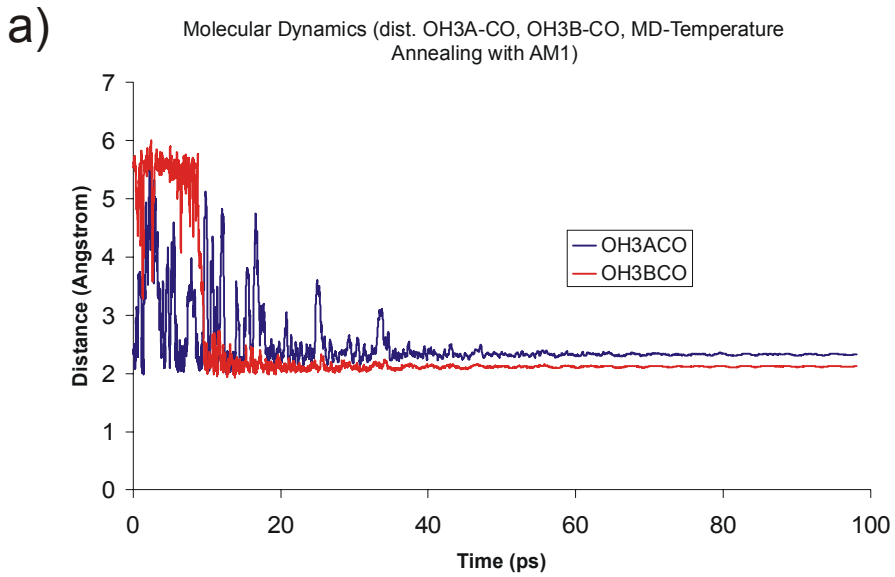

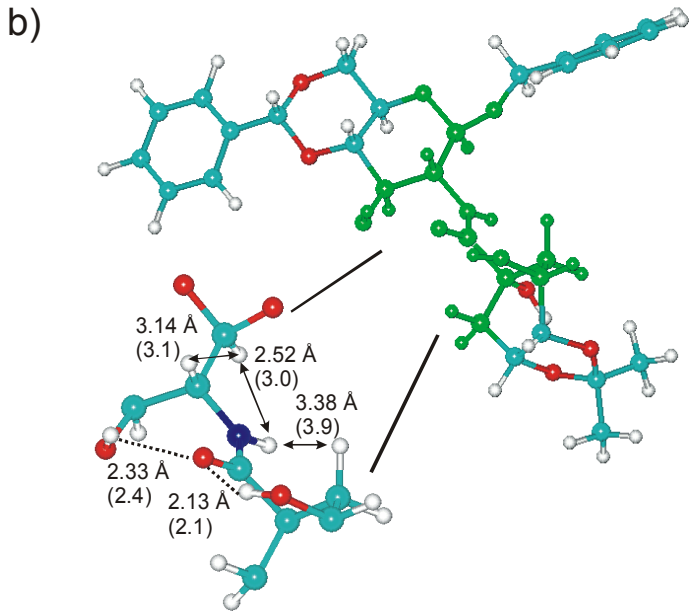

Figure 5. (a) *Inter*-proton distance for $OH3^A$ and $OH3^B$ hydrogen-bonded, respectively, to the amide carbonyl from the 150 ps trajectory of **6b** during temperature annealing from 600 K to 0 K; (b) Lowest energy structure for **6b** with selected 0 K distances. High-temperature average distances from the first 30 ps of the trajectory are shown in parentheses.

The observed NOE enhancements between both $H6b^B$/NH and $H2b^B$/NH (not shown) were fully consistent with the relative positions of ring A and B. The hydrogen bonding network across the amide bond appears to be only minimally influenced by the anomeric configurations in **6a** and **6b** and the steric demand of the benzyl group. Unlike **6a**, the hydroxyl groups in **6b** did not display any long-range NOEs, which implies a stronger *intra*-molecular H-bond network that is affected less by water present in $CDCl_3$. Traces of water were present in both NMR samples at the time of analysis (signal at 1.5 ppm in $CDCl_3$). For **6b**, only a weak negative NOE was observed between the hydroxyl resonances at 2.9 and 3.0 ppm.[13] These are presumably $OH3^A$ and $OH3^B$ hydrogen-bonded to the amide carbonyl oxygen; however, unequivocal identification was not possible.

The lowest-energy conformation of the quinamide cluster **16** after temperature annealing was fully consistent with the experimental NMR data and is shown in Figure 6a. The equatorial position of OH2 in ring A allowed the formation of a hydrogen bond towards the amide carbonyl oxygen in addition to the hydrogen bond between $OH3^B$ and the same carbonyl. The amide NH-group was hydrogen bonded to $OH1^B$, which in turn formed a weak hydrogen bond towards the isopropylidene acetal oxygen at $C5^B$. The so-obtained *twist*-boat conformation in ring B was identical to that found in the model compound **8**.

Unlike compound **16**, the quinic carboxamide **17** displayed the amide linkage at $C2^A$ and the OH-group at $C3^A$ in diaxial positions unsuitable for mutual hydrogen bonding. The conformation

of the amide linkage was supported by an experimental NOE at the amide NH-proton after irradiation of $H4^{A}$ (inset in Figure 6b).

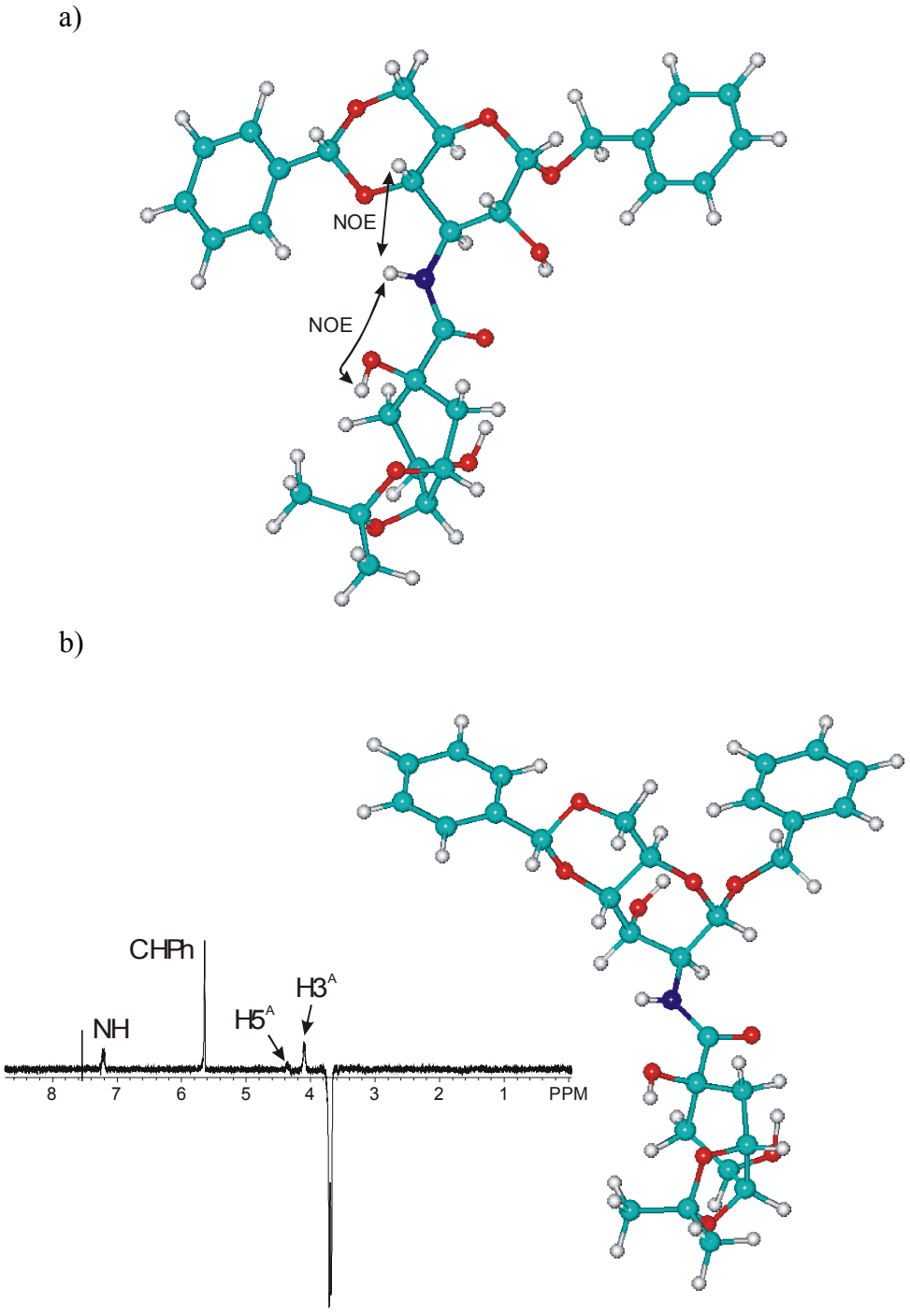

Figure 6. Temperature annealed lowest energy structures *in vacuo*. a) Compound **16**. The conformation of the amide linkage was confirmed through an NOE between NH, $H3^{A}$ and $OH1^{B}$; b) **17**. The conformation of the amide linkage in **17** was confirmed through a strong NOE

between NH, $H4^A$, and $OH1^B$. The NOE difference spectrum after irradiation of $H4^A$ is shown as inset.

In this investigation, the solution structures of three quinic amide derivatives in $CDCl_3$ were solved. For all three carboxamides, NOE signal buildup within rings A/B and across the amide bond was found fully supported by accompanying molecular dynamics calculations *in vacuo*. Unusually strong spin density exchange between all OH-protons and remote ring protons was interpreted as evidence for hydration in the compounds **6**, **16**, and **17**. In the β-anomer of **6**, spin exchange between the hydroxyl groups was less pronounced. The cyclohexane *twist*-boat conformation was shown to be the result of the cyclic five-membered acetal and trans-annular hydrogen bonding. The *twist*-boat conformation was found to exist even in the simple unsubstituted quinic carboxamide **8**. We are currently synthesizing analogs with different stereochemistries for structural comparison and for evaluation of biological activity.

Experimental Section

General Procedures. **NOEDIF experiments.** Approximately 10 mg of the compound was dissolved in $CDCl_3$ and was subjected to three freeze-thaw cycles in liquid nitrogen with evacuation/N_2-flushing on a Schlenk line while frozen. NOEDIF spectra were recorded non-spinning for 512 transients at room temperature on a 300 MHz Varian Mercury system. An array of eight different mixing times between $0.5*10^{-3}$ s and $3*10^{-3}$ s yielded spectra whose NOE signals were integrated relative to the negative irradiated proton signal, and the resulting integrated NOE signal intensity values were plotted against the mixing time. With the first three or four data points, a linear buildup curve was constructed for the respective proton pair. The slope from the benzylidene/$H6a^A$ proton pair (slope = $0.035*10^{-3}$ s^{-1} and $0.023*10^{-3}$ s^{-1} for **6a** and **6b**, respectively) in the rigid ring A was used as a reference slope. All other experimental buildup slopes were brought in relation to the reference slope and the respective *inter*-proton distances from molecular modeling by equation (1).

Molecular dynamics

The molecule was constructed in HyperChem 5.1. Ring B was constructed in the *twist*-boat conformation, and two dihedral angles were restrained to maintain the *twist*-boat conformation during the dynamics simulation. The compound was initially constructed with protons oriented to match NOE information. The structure was energy minimized with molecular mechanics (MM+ force field) followed by the semi-empirical AM1-method. The molecule was subsequently modeled with molecular dynamics (T_{init} = 280 K, T_{simul} = 600 K, T_{final} = 0 K, temperature steps = 10 K, heat time = 0.5 ps, run time = 100 ps, cool time = 0.5 ps, step size = 0.1 fs). Data from dihedral angles or *inter*-proton distances were collected in a snapshot file at every 100 time steps, i.e. every 10 fs.

5,7-Dihydroxy-2,2-dimethyl-hexahydro-benzo[1,3]dioxole-5-carboxylic acid amide (8). Quinic lactone **7** (0.50 g, 2.4 mmol) was suspended in MeOH (40 mL) and concentrated NH_4OH (1 mL) and was heated at 90 ºC for 24 h in a stainless steel autoclave pressurized with NH_3-gas to 80 psi. The vessel was cooled to rt, and the colorless solution was evaporated to dryness. The colorless crystals were NMR-pure. Yield (0.51 g, 2.2 mmol, 95 %), mp 136-138 ºC, TLC R_f 0.5 (EtOAc:EtOH 9:1), ESI-MS $[M+H]^+$ *m/z* 232.4, theor. *m/z* 232.1 ($C_{10}H_{17}NO_5$), high mass accuracy reflectron TOF-MS $[M+H]^+$ *m/z* 232.1342 (error: 15 mDa), IR (cm^{-1}): 3408.2, 3296.4, 3014.7, 2978.1, 2939.5, 2899.0, 1681.9, 1651.1, 1240.2, 1128.4, 1051.2, ^{13}C-NMR: ($CDCl_3$, in ppm) δ 24.37, 27.06, 34.23, 36.97, 65.90, 72.10, 76.04, 108.75, 179.51, $C_{10}H_{17}O_5N_{theor}$ C 51.92 %, H 7.41 %, N 6.06 % $C_{10}H_{17}O_5N_{found}$ C 51.88 %, H 7.33 %, N 6.11 %.

Benzyl-3-amino-4,6-*O*-benzylidene-3-deoxy-*N*-[5,7-dihydroxy-2,2-dimethyl-hexahydro-benzo[1,3]dioxole-5-oyl]-α-D-glucopyranoside (16) and benzyl-2-amino-4,6-*O*-benzylidene-2-deoxy-*N*-[5,7-dihydroxy-2,2-dimethyl-hexahydro-benzo[1,3]dioxole-5-oyl]-α-D-altropyranoside (17). Quinic lactone **7** (0.5 g, 2.4 mmol) was dissolved in *N,N*-dimethylacetamide (1 mL) along with a mixture (0.9 g, 2.5 mmol) of benzyl-3-amino-4,6-*O*-benzylidene-3-deoxy-α-D-glucopyranoside **14** and benzyl-2-amino-4,6-*O*-benzylidene-2-deoxy-α-D-altropyranoside **15**. The mixture of aminosugars was obtained from a published procedure[15] in a ratio **14**:**15** of 1:20 by NMR. The solution was heated to 70 ºC for 3 d during which a crystalline precipitate formed. The solution was digested with Et_2O (20 mL), and the crude product was filtered off. Compounds **16** and **17** were separated by silica gel chromatography (EtOAc).

16. Yield (50 mg, 0.087 mmol, 70 %), mp 218-220 ºC (partial decomposition), TLC R_f 0.57 (EtOAc), MS $[M+H]^+$ *m/z* 572.21, theor. *m/z* 572.24 ($C_{30}H_{37}NO_{10}+H^+$), high mass accuracy reflectron TOF-MS $[M+H]^+$ *m/z* 572.2479 (error: 1.2 mDa), ^{13}C-NMR: (in ppm) δ 24.53, 27.20, 29.92, 34.57, 37.25, 53.47, 63.91, 66.02, 69.13, 70.50, 72.13, 72.27, 73.28, 76.08, 78.56, 98.42, 101.75, 108.90, 126.25, 128.40, 128.49, 128.82, 129.30, 136.90, 137.14, 178.74, $C_{30}H_{37}O_{10}N_{theor}$ C 63.01 %, H 6.53 %, N 2.45 % $C_{30}H_{37}O_{10}N_{found}$ C 62.93 %, H 6.44 %, N 2.38 %.

17. Yield (960 mg, 1.7 mmol, 70 %), mp 105-107 ºC (partial decomposition), TLC R_f 0.7 (EtOAc), MS $[M+H]^+$ *m/z* 572.19, theor. *m/z* 572.24 ($C_{30}H_{37}NO_{10}+H^+$), high mass accuracy reflectron TOF-MS $[M+H]^+$ *m/z* 572.2484 (error: 1.0 mDa), ^{13}C-NMR: (in ppm) δ 24.67, 27.32, 29.93, 34.34, 37.55, 52.05, 58.91, 66.27, 67.89, 69.22, 70.40, 72.43, 73.37, 76.36, 98.89, 102.61, 109.08, 126.46, 128.43, 128.54, 128.90, 129.47, 136.33, 137.17, 176.05, $C_{30}H_{37}O_{10}N_{theor}$ C 63.01 %, H 6.53 %, N 2.45 % $C_{30}H_{37}O_{10}N_{found}$ C 62.90 %, H 6.46 %, N 2.41 %.

Acknowledgements

The authors thank the Department of Chemistry for financial support and Teresa Vail for valuable discussions. A. H. F. acknowledges the College of the Pacific for an Eberhardt Research Fellowship.

References and Notes

1. Fischer, H. O. L. *Ber.*, **1921**, *54B*, 775.
2. Fischer, H. O. L.; Dangschat, G. *Helv. Chim. Acta*, **1934**, *17*, 1200.
3. Fischer, H. O. L.; Dangschat, G. *Helv. Chim. Acta*, **1935**, *18*, 1206.
4. Fischer, H. O. L.; Dangschat, G. *Helv. Chim. Acta*, **1935**, *18*, 1204.
5. Jiang, S.; Singh, G. *Tetrahedron*, **1998**, *54*, 4697.
6. Herrmann, K. M.; Weaver, L. M. *Annu. Rev. Plant Physiol. Plant Mol. Biol.*, **1999**, *50*, 473.
7. Sanchez-Sixto, C.; Prazeres, V. F. V.; Castedo, L.; Lamb, H.; Hawkins, A. R.; Gonzalez-Bello, C. *J. Med. Chem.*, **2005**, *48*, 4871.
8. Eisenberg, E. J.; Bidgood, A.; Coundy, K. C. *Antimicrob. Agents Chemother.*, **1997**, *41*, 1949.
9. Kim, C. U.; Lew, W.; Williams, M. A.; Zhang, L.; Liu, H.; Swaminathan, S.; Bischofberger, N.; Chen, M. S.; Tai, C. Y.; Mendel, D. B.; Laver, W. G.; Stevens, R. C. *J. Am. Chem. Soc.*, **1997**, *119*, 681.
10. Bischofberger, N. W.; Kim, C. U.; Lew, W.; Liu, H.; Williams, M. A. *PCT Int. Appl.*; (Gilead Sciences, Inc., USA)., 1996.Farina, V.; Brown, J. D. *Angew. Chem., Int. Ed.*, **2006**, *45*, 7330.
11. Ward, P.; Small, I.; Smith, J.; Suter, P.; Dutkowski, R. *J. Antimicrob. Chemother.*, **2005**, *55*, i5.
12. Nguyen, T. T. M.; Gross, P. H.; Franz, A. H. *ARKIVOC (Gainesville, FL, United States)*, **2005**, 110.
13. Trost, B. M.; Romero, A. G. *J. Org. Chem.*, **1986**, *51*, 2332.
14. Chiu, T. K.; Sigillo, K.; Gross, P. H.; Franz, A. H. *Synth. Commun.* **2007**, *37* (14), 2355-2381.
15. Myers, W. H.; Robertson, G. J. *J. Am. Chem. Soc.*, **1943**, *65*, 8.
16. Fuerst, A.; Plattner, P. A. *12th Int. Congress Pure Appl. Chem.* New York, 1951.
17. Newth, F. H. *Quart. Revs. (London)*, **1959**, *13*, 30.